



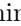



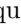
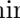



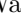


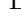

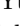
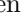
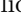
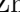
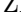





A model-agnostic likelihood for the reinterpretation of the $B^+ \rightarrow K^+ \nu \bar{\nu}$ measurement at Belle II

M. Abumusabh[✉], I. Adachi[✉], L. Aggarwal[✉], H. Ahmed[✉], Y. Ahn[✉], N. Akopov[✉], S. Alghamdi[✉], M. Alhakami[✉],
A. Aloisio[✉], N. Althubiti[✉], K. Amos[✉], N. Anh Ky[✉], D. M. Asner[✉], H. Atmacan[✉], R. Ayad[✉], V. Babu[✉],
H. Bae[✉], N. K. Baghel[✉], P. Bambade[✉], Sw. Banerjee[✉], M. Barrett[✉], M. Bartl[✉], J. Baudot[✉], A. Baur[✉],
A. Beaubien[✉], F. Becherer[✉], J. Becker[✉], J. V. Bennett[✉], F. U. Bernlochner[✉], V. Bertacchi[✉], M. Bertemes[✉],
E. Bertholet[✉], M. Bessner[✉], S. Bettarini[✉], V. Bhardwaj[✉], B. Bhuyan[✉], F. Bianchi[✉], D. Biswas[✉], D. Bodrov[✉],
A. Bondar[✉], G. Bonvicini[✉], J. Borah[✉], A. Boschetti[✉], A. Bozek[✉], M. Bračko[✉], P. Branchini[✉], T. E. Browder[✉],
A. Budano[✉], S. Bussino[✉], Q. Campagna[✉], M. Campajola[✉], L. Cao[✉], G. Casarosa[✉], C. Cecchi[✉], M.-C. Chang[✉],
P. Cheema[✉], L. Chen[✉], B. G. Cheon[✉], K. Chilikin[✉], J. Chin[✉], K. Chirapatpimol[✉], H.-E. Cho[✉], K. Cho[✉],
S.-J. Cho[✉], S.-K. Choi[✉], S. Choudhury[✉], L. Corona[✉], J. X. Cui[✉], E. De La Cruz-Burelo[✉], S. A. De La Motte[✉],
G. de Marino[✉], G. De Nardo[✉], G. De Pietro[✉], R. de Sangro[✉], M. Destefanis[✉], S. Dey[✉], J. Dingfelder[✉],
Z. Doležal[✉], T. V. Dong[✉], X. Dong[✉], K. Dugic[✉], G. Dujany[✉], P. Ecker[✉], R. Farkas[✉], T. Ferber[✉], T. Fillinger[✉],
C. Finck[✉], G. Finocchiaro[✉], F. Forti[✉], A. Frey[✉], B. G. Fulsom[✉], A. Gabrielli[✉], A. Gale[✉], E. Ganiev[✉],
M. Garcia-Hernandez[✉], R. Garg[✉], L. Gärtner[✉], G. Gaudino[✉], V. Gaur[✉], V. Gautam[✉], A. Gellrich[✉],
D. Ghosh[✉], H. Ghumaryan[✉], G. Giakoustidis[✉], R. Giordano[✉], A. Giri[✉], P. Gironella Gironell[✉], B. Gobbo[✉],
R. Godang[✉], P. Goldenzweig[✉], W. Gradl[✉], E. Graziani[✉], D. Greenwald[✉], K. Gudkova[✉], I. Haide[✉], Y. Han[✉],
C. Harris[✉], H. Hayashii[✉], S. Hazra[✉], C. Hearty[✉], M. T. Hedges[✉], G. Heine[✉], I. Heredia de la Cruz[✉],
T. Higuchi[✉], M. Hoek[✉], M. Hohmann[✉], R. Hoppe[✉], P. Horak[✉], X. T. Hou[✉], C.-L. Hsu[✉], T. Humair[✉],
T. Iijima[✉], K. Inami[✉], N. Ipsita[✉], A. Ishikawa[✉], R. Itoh[✉], M. Iwasaki[✉], P. Jackson[✉], D. Jacobi[✉],
W. W. Jacobs[✉], E.-J. Jang[✉], Y. Jin[✉], A. Johnson[✉], K. K. Joo[✉], M. Kaleta[✉], J. Kandra[✉], K. H. Kang[✉],
G. Karyan[✉], F. Keil[✉], C. Kiesling[✉], C.-H. Kim[✉], D. Y. Kim[✉], J.-Y. Kim[✉], K.-H. Kim[✉], H. Kindo[✉],
K. Kinoshita[✉], P. Kodyš[✉], T. Koga[✉], S. Kohani[✉], K. Kojima[✉], A. Korobov[✉], S. Korpar[✉], E. Kovalenko[✉],
R. Kowalewski[✉], P. Križan[✉], P. Krokovny[✉], T. Kuhr[✉], Y. Kulii[✉], J. Kumar[✉], R. Kumar[✉], K. Kumara[✉],
T. Kunigo[✉], A. Kuzmin[✉], Y.-J. Kwon[✉], K. Lalwani[✉], T. Lam[✉], J. S. Lange[✉], T. S. Lau[✉], M. Laurenza[✉],
R. Lebouchier[✉], F. R. Le Diberder[✉], M. J. Lee[✉], C. Lemettais[✉], P. Leo[✉], C. Li[✉], H.-J. Li[✉], L. K. Li[✉],
Q. M. Li[✉], W. Z. Li[✉], Y. Li[✉], Y. B. Li[✉], Y. P. Liao[✉], J. Libby[✉], J. Lin[✉], S. Lin[✉], M. H. Liu[✉], Q. Y. Liu[✉],
Z. Liu[✉], D. Liventsev[✉], S. Longo[✉], A. Lozar[✉], T. Lueck[✉], C. Lyu[✉], Y. Ma[✉], M. Maggiora[✉], S. P. Maharana[✉],
R. Maiti[✉], G. Mancinelli[✉], R. Manfredi[✉], E. Manoni[✉], M. Mantovano[✉], D. Marcantonio[✉], S. Marcello[✉],
C. Marinas[✉], C. Martellini[✉], A. Martens[✉], T. Martinov[✉], L. Massaccesi[✉], M. Masuda[✉], K. Matsuoka[✉],
D. Matvienko[✉], S. K. Maurya[✉], M. Maushart[✉], J. A. McKenna[✉], Z. Mediankin Gruberová[✉], R. Mehta[✉],
F. Meier[✉], D. Meleshko[✉], M. Merola[✉], C. Miller[✉], M. Mirra[✉], K. Miyabayashi[✉], H. Miyake[✉], S. Mondal[✉],
S. Moneta[✉], A. L. Moreira de Carvalho[✉], H.-G. Moser[✉], R. Mussa[✉], I. Nakamura[✉], M. Nakao[✉], H. Nakazawa[✉],
Y. Nakazawa[✉], Z. Natkaniec[✉], A. Natchii[✉], M. Nayak[✉], M. Neu[✉], S. Nishida[✉], S. Ogawa[✉], R. Okubo[✉],
H. Ono[✉], Y. Onuki[✉], G. Pakhlova[✉], S. Pardi[✉], J. Park[✉], S.-H. Park[✉], S. Patra[✉], S. Paul[✉], T. K. Pedlar[✉],
R. Pestotnik[✉], L. E. Piilonen[✉], P. L. M. Podesta-Lerma[✉], T. Podobnik[✉], C. Praz[✉], S. Prell[✉], E. Prencipe[✉],
M. T. Prim[✉], S. Privalov[✉], H. Purwar[✉], P. Rados[✉], G. Raeuber[✉], S. Raiz[✉], V. Raj[✉], K. Ravindran[✉],
J. U. Rehman[✉], M. Reif[✉], S. Reiter[✉], D. Ricalde Herrmann[✉], I. Ripp-Baudot[✉], G. Rizzo[✉], S. H. Robertson[✉],
J. M. Roney[✉], A. Rostomyan[✉], N. Rout[✉], L. Salutati[✉], D. A. Sanders[✉], S. Sandilya[✉], L. Santelj[✉], C. Santos[✉],
V. Savinov[✉], B. Scavino[✉], C. Schmitt[✉], M. Schnepf[✉], K. Schoenning[✉], C. Schwanda[✉], Y. Seino[✉], A. Selce[✉],
K. Senyo[✉], J. Serrano[✉], M. E. Sevir[✉], C. Sfienti[✉], W. Shan[✉], X. D. Shi[✉], T. Shillington[✉], T. Shimasaki[✉],
J.-G. Shiu[✉], D. Shtol[✉], A. Sibidanov[✉], F. Simon[✉], J. B. Singh[✉], J. Skorupa[✉], R. J. Sobie[✉], M. Sobotzik[✉],
A. Soffer[✉], A. Sokolov[✉], E. Solovieva[✉], S. Spataro[✉], B. Spruck[✉], M. Starič[✉], P. Stavroulakis[✉], S. Stefkova[✉],

L. Stoetzer , R. Stroili , M. Sumihama , N. Suwonjandee , H. Svidras , M. Takizawa , S. Tanaka ,
 S. S. Tang , K. Tanida , F. Tenchini , F. Testa , A. Thaller , O. Tittel , R. Tiwary , E. Torassa ,
 F. F. Trantou , I. Tsaklidis , I. Ueda , K. Unger , Y. Unno , K. Uno , S. Uno , P. Urquijo , Y. Ushiroda ,
 S. E. Vahsen , R. van Tonder , K. E. Varvell , M. Veronesi , V. S. Vismaya , L. Vitale , R. Volpe ,
 M. Wakai , S. Wallner , M.-Z. Wang , X. L. Wang , A. Warburton , C. Wessel , B. D. Yabsley ,
 S. Yamada , W. Yan , S. B. Yang , J. Yelton , J. H. Yin , K. Yoshihara , B. Yu , C. Z. Yuan , J. Yuan ,
 Y. Yusa , L. Zani , F. Zeng , B. Zhang , V. Zhilich , J. S. Zhou , Q. D. Zhou , L. Zhu , and R. Žlebčák 
 (The Belle II Collaboration)

We recently measured the branching fraction of the $B^+ \rightarrow K^+ \nu \bar{\nu}$ decay using 362 fb^{-1} of on-resonance e^+e^- collision data, under the assumption of Standard Model kinematics, providing the first evidence for this decay. To facilitate future reinterpretations and maximize the scientific impact of this measurement, we hereby publicly release the full analysis likelihood along with all necessary material required for reinterpretation under arbitrary theoretical models sensitive to this measurement. In this work, we demonstrate how the measurement can be reinterpreted within the framework of the Weak Effective Theory. Using a kinematic reweighting technique in combination with the published likelihood, we derive marginal posterior distributions for the Wilson coefficients, construct credible intervals, and assess the goodness of fit to the Belle II data. For the Weak Effective Theory Wilson coefficients, the posterior mode of the magnitudes $|C_{\text{VL}} + C_{\text{VR}}|$, $|C_{\text{SL}} + C_{\text{SR}}|$, and $|C_{\text{TL}}|$ corresponds to the point (11.3, 0.00, 8.21). The respective 95% credible intervals are [1.86, 16.2], [0.00, 15.4], and [0.00, 11.2].

Measurements are typically performed under the assumptions of a specific theoretical model, but have the potential to constrain a large variety of additional models. Reinterpretations neglecting variations in detector efficiency, at scales below the provided resolution, can introduce biases. More robust alternatives typically require access to the full analysis strategy and the computationally intensive event simulation, or the ability to perform event-level reweighting using the original analysis samples – which are usually not publicly accessible. The method introduced in Ref. [1] offers an efficient approach to reinterpret measurements in terms of alternative theoretical models, while accurately accounting for efficiency variations at high resolution. The key advantage of this method lies in its ability to construct and publish a reinterpretable, *model-agnostic*, likelihood, which enables the assessment of data compatibility with a wide range of theoretical models. In this work, we provide the necessary information to apply this method to our $B^+ \rightarrow K^+ \nu \bar{\nu}$ result [2] and demonstrate its potential using a selected alternative model.

Flavor-changing neutral-current $b \rightarrow s \nu \bar{\nu}$ transitions are suppressed in the Standard Model (SM) of particle physics due to the Glashow-Iliopoulos-Maiani mechanism [3]. The branching fraction of the exclusive $b \rightarrow s \nu \bar{\nu}$ process, $B^+ \rightarrow K^+ \nu \bar{\nu}$ decay,¹ is predicted in the SM to be [4]

$$\mathcal{B}(B^+ \rightarrow K^+ \nu \bar{\nu}) = (5.58 \pm 0.37) \cdot 10^{-6}, \quad (1)$$

which includes a contribution of $(0.61 \pm 0.06) \cdot 10^{-6}$ from the long-distance double-charged-current $B^+ \rightarrow \tau^+(\rightarrow K^+ \bar{\nu}_\tau) \nu_\tau$ decay. Since the B meson is a pseudoscalar, the decay is isotropic in its rest frame.

Hence, the only experimentally accessible kinematic degree of freedom is the squared dineutrino invariant mass, $q^2 = (p_\nu + p_{\bar{\nu}})^2 = (p_B - p_K)^2$, a key variable in probing new physics (NP) beyond the SM. The differential branching fraction $d\mathcal{B}/dq^2$ is directly proportional to the squared $B \rightarrow K$ transition form factor, $|f_+(q^2)|^2$, and the phase-space factor. The largest theoretical uncertainty in the SM prediction stems from imprecise knowledge of $f_+(q^2)$, which is parametrized by 3 hadronic parameters.

The $B^+ \rightarrow K^+ \nu \bar{\nu}$ decay has been studied by the CLEO, BABAR, Belle, and Belle II collaborations [2, 5–10], with the latest measurement by the Belle II collaboration finding the first evidence for this decay at 3.5 standard deviations. This result, based on the SM prediction from Ref. [4] and hadronic parameters from the HPQCD collaboration [11] as a model ansatz, exceeds the SM expectation by 2.7 standard deviations. This enhanced branching fraction triggered the high-energy physics community to interpret this result under different NP scenarios [12–14]. However, such reinterpretations are only approximate as not all relevant information on the measurement was previously accessible to the public.

Generally, two distinct classes of NP models can replicate the signature of a $B^+ \rightarrow K^+ \nu \bar{\nu}$ decay. These models naturally mimic the neutrino pair in the final state of $B^+ \rightarrow K^+ \nu \bar{\nu}$ decays, as the neutrinos remain undetected at Belle II. NP scenarios can proceed via either three-body or two-body decays. In three-body decays, the properties of NP can be studied within the framework of the Weak Effective Theory (WET). This is an effective quantum field theory that describes both the SM and potential NP effects within a common parameter framework, where NP particles and force carriers have masses at or above the electroweak symmetry-breaking scale. Examples of such models include leptoquarks [15]

¹ Charge-conjugate channels are implied throughout this work.

and heavy Z' bosons [16]. Two-body decays would signal the presence of light NP, which lies below the scale of electroweak symmetry breaking, and is not described by the WET. Explicit examples include axion-like particles [17] or other dark-sector mediators [18].

The primary goals of this work are twofold: to publish the model-agnostic likelihood for the $B^+ \rightarrow K^+ \nu \bar{\nu}$ analysis; and to reinterpret the result in the framework of the WET, providing constraints on relevant Wilson coefficients. This work includes: a summary of the most relevant aspects of the $B^+ \rightarrow K^+ \nu \bar{\nu}$ analysis [2]; a description of the kinematic reweighting method used for reinterpretation; details of the statistical inference procedure; results for the WET reinterpretation; and comparisons of model fit quality and relative performance with respect to the SM and background-only hypotheses.

The Belle II analysis of $B^+ \rightarrow K^+ \nu \bar{\nu}$ decays [2], originating from a $e^+e^- \rightarrow \Upsilon(4S) \rightarrow B^+B^-$ process, was performed using two different reconstruction methods: the more sensitive *inclusive* tagging analysis (ITA) and the more conventional *hadronic* tagging analysis (HTA), targeting nearly orthogonal datasets. In the HTA, we reconstruct the non-signal B meson of the B^+B^- pair in specific hadronic decay modes. Further, the signal B meson is reconstructed, providing a well-constrained event topology with low background but limited efficiency. In contrast, in the ITA, we identified the signal by reconstructing the K^+ track, summing all visible particles in the event, and then inferring the missing energy. Thereby, we achieved higher sensitivity, though at the cost of increased background contamination. In addition to a basic preselection, the ITA (HTA) used two (one) boosted decision trees, BDT_1 and BDT_2 (BDTh) to separate the signal from the background. The statistical model was constructed using Monte Carlo simulated data for the signal and seven background categories: decays of charged and neutral $B\bar{B}$ mesons; continuum processes ($u\bar{u}$, $d\bar{d}$, $s\bar{s}$, $c\bar{c}$); and low-multiplicity $\tau^+\tau^-$ backgrounds. In this measurement, only the short-distance contribution was considered as signal, with a corresponding branching fraction of $(4.97 \pm 0.37) \cdot 10^{-6}$ [4].

For both the ITA and HTA methods, a binned Poissonian likelihood was constructed using the `HistFactory` statistical model [19], implemented in the `pyhf` framework [20, 21], incorporating all systematic uncertainties. The ITA analysis used 4×3 bins in the $\eta(\text{BDT}_2) \times q_{\text{rec}}^2$ space, where $\eta(\text{BDT}_2)$ is the transformed BDT_2 output, such that each bin represents a 2% efficiency quantile for the selection, and q_{rec}^2 is the reconstructed q^2 . The latter is defined as $q_{\text{rec}}^2 = s/4 + M_K^2 - \sqrt{s}E_K^*$, where \sqrt{s} is the center of mass energy, M_K is the nominal kaon mass and E_K^* is the reconstructed energy of the kaon in the collision center of mass frame. The ITA and HTA q^2 resolutions are approximately 1 GeV^2 and 0.3 GeV^2 , respectively, leading to differences in the q_{rec}^2 and q^2 distributions.² We note that final state radiation has a neg-

ligible effect on the presented results. The ITA includes both a signal and a control region, resulting in a total of 24 reconstruction bins. Signal region bins are populated with events that pass all selection criteria in 362 fb^{-1} of on-resonance data, taken at a center of mass energy of $\sqrt{s} \approx 10.58 \text{ GeV}$, which corresponds to the $\Upsilon(4S)$ resonance. Control region bins are filled with events that pass the same selection in 42 fb^{-1} of off-resonance data, taken at $\sqrt{s} \approx 10.52 \text{ GeV}$. The control region improves constraints on the background contributions from continuum processes. The HTA used 6 bins in the $\eta(\text{BDTh})$ space. These bins contain only events that pass all selection criteria in 362 fb^{-1} of on-resonance data.

The ITA and HTA likelihoods were combined into one likelihood, accounting for the correlations between the systematic uncertainties in the two methods. The *combined* likelihood includes 231 nuisance parameters χ , in addition to one parameter of interest, the signal strength $\eta = [\mu_{\text{SM}}]$, which represents the signal branching fraction relative to its SM expectation. A maximum likelihood fit yielded a signal strength of $\mu_{\text{SM}} = 4.6 \pm 1.3$, which corresponds to a branching fraction of $(2.3 \pm 0.5(\text{stat})_{-0.4}^{+0.5}(\text{syst})) \cdot 10^{-5}$. This result has a significance of 3.5 standard deviations over the background-only hypothesis and a significance of 2.7 standard deviations over the SM hypothesis. The combined likelihood serves as the basis for reinterpretation in this study.

For the reinterpretation of such a SM-dependent template likelihood, an alternative signal template must be derived from the corresponding theoretical prediction, while ensuring consistency with the experimental acceptance. This is enabled by the reinterpretation method introduced in Ref. [1], which allows the construction of a model-agnostic likelihood from the published $B^+ \rightarrow K^+ \nu \bar{\nu}$ likelihood [2] using histogram reweighting. The key innovation of this method lies in its ability to capture the effect of reweighting a measured observable distribution based on a parametrized theoretical distribution without requiring access to event-level Monte Carlo information.

The number density of expected events after all selections, given a theoretical prediction of the cross section density $\sigma(q^2)$ for a reconstruction (fitting) variable x reads

$$n(x) = L \int dq^2 \varepsilon(x|q^2) \sigma(q^2) = \int dq^2 n(x, q^2), \quad (2)$$

where reconstruction and selection efficiency is combined into $\varepsilon(x|q^2)$, L is the total integrated luminosity, and $n(x, q^2) \equiv L \varepsilon(x|q^2) \sigma(q^2)$ is defined as the joint number density. For a reinterpretation, it is necessary to determine the number density $n_1(x)$ of an *alternative* theoretical prediction $\sigma_1(q^2)$, starting from the joint number density $n_0(x, q^2)$, based on a kinematic *null* distribution $\sigma_0(q^2)$. This can be obtained by weighting,

$$n_1(x) = \int dq^2 n_0(x, q^2) w(q^2), \quad (3)$$

² We set $c = 1$ throughout this work.

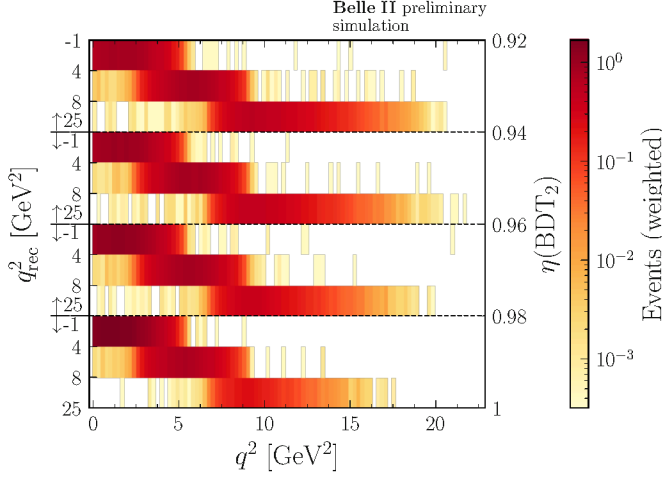


Figure 1. The ITA binned joint number densities. The horizontal axis corresponds to the generated q^2 . The vertical axis represents the binning used in the $B^+ \rightarrow K^+ \nu \bar{\nu}$ analysis [2]. The heatmap shows the weighted signal events.

with the weight factor $w(q^2) = \sigma_1(q^2)/\sigma_0(q^2)$. For an application to a binned likelihood, such as the $B^+ \rightarrow K^+ \nu \bar{\nu}$ likelihood [2], the reweighting step of Eq. (3) becomes

$$n_{1,x} = \sum_{q^2 \text{ bins}} n_{0,xq^2} w_{q^2}, \quad (4)$$

where the subscripts represent bin indices. The discrete joint number density n_{0,xq^2} and weights $w_{q^2} = \sigma_{1,q^2}/\sigma_{0,q^2}$ can be obtained from the continuous counterparts by integrating over the corresponding bin intervals, as detailed in Ref. [1]. This reweighting process only requires knowledge of the joint null number density n_{0,xq^2} , the basis of the model-agnostic likelihood. Together with the weight factor w_{q^2} , this is sufficient information to predict the number density based on any alternative theory, enabling the statistical inference of relevant parameters. This reinterpretation method, integrated within the **pyhf** framework [20, 21], is implemented in the **redist** software [22].

To obtain the joint number density n_{0,xq^2} , we use simulated SM signal events from the $B^+ \rightarrow K^+ \nu \bar{\nu}$ analysis [2], satisfying all selection criteria. These include information on the generated and reconstructed squared momenta, q^2 and q_{rec}^2 , as well as the classifier responses $\eta(\text{BDT}_2)$ and $\eta(\text{BDTh})$. The number of q^2 bins for n_{0,xq^2} is determined by the differences between the null and the anticipated alternative distributions. The null distribution is the $B^+ \rightarrow K^+ \nu \bar{\nu}$ SM prediction based on the form factors from Ref. [11]. The WET predicts a broad distribution in q^2 . With future studies in mind, the binning strategy is optimized to capture localized features in the q^2 spectrum, resulting in 100 equally spaced q^2 bins in the kinematically allowed region plus one negative q^2 bin for events falling outside of this region. An example of n_{0,xq^2} for the ITA is shown in Fig. 1.

In this reinterpretation study, we build on the **HistFactory** likelihood [19], to construct a Bayesian pos-

terior for parameter inference. Starting from the likelihood,

$$p(\mathbf{n}, \mathbf{a} | \boldsymbol{\eta}, \boldsymbol{\chi}) = p(\mathbf{n} | \boldsymbol{\eta}, \boldsymbol{\chi}) p(\mathbf{a} | \boldsymbol{\chi}), \quad (5)$$

with observed and auxiliary data, \mathbf{n}, \mathbf{a} , respectively, and unconstrained parameters of interest $\boldsymbol{\eta}$ and constrained nuisance parameters $\boldsymbol{\chi}$, we construct the posterior model

$$p(\boldsymbol{\eta}, \boldsymbol{\chi} | \mathbf{n}, \mathbf{a}) \propto p(\mathbf{n} | \boldsymbol{\eta}, \boldsymbol{\chi}) p(\boldsymbol{\chi} | \mathbf{a}) p(\boldsymbol{\eta}). \quad (6)$$

The likelihood for constraining nuisance parameters with auxiliary data, $p(\mathbf{a} | \boldsymbol{\chi})$, is translated into a prior for all constrained parameters $p(\boldsymbol{\chi} | \mathbf{a}) \propto p(\mathbf{a} | \boldsymbol{\chi}) p(\boldsymbol{\chi})$ with a normally distributed initial prior $p(\boldsymbol{\chi})$, as detailed in Ref. [23]. Additionally, a prior for unconstrained parameters $p(\boldsymbol{\eta})$ is introduced. The **bayesian pyhf** framework [23] implements the posterior, using **pymc** [24] as a back-end for sampling.

A commonly-used framework to describe NP scenarios without using a UV-complete theoretical model is the WET. Following Ref. [1], we consider six local operators of mass dimension six [25], where we assume massless neutrinos and consider operators as sums over neutrino flavors. The resulting differential branching fraction for $B^+ \rightarrow K^+ \nu \bar{\nu}$ as predicted by the WET is given by [25, 26]

$$\begin{aligned} \frac{d\mathcal{B}}{dq^2} = & 3\tau_B \left(\frac{4G_F}{\sqrt{2}} \frac{\alpha}{2\pi} \right)^2 |V_{ts}^* V_{tb}|^2 \frac{\sqrt{\lambda_{BK}} q^2}{(4\pi)^3 M_B^3} \\ & \cdot \left[\frac{\lambda_{BK}}{24q^2} |f_+(q^2)|^2 |C_{\text{VL}} + C_{\text{VR}}|^2 \right. \\ & + \frac{(M_B^2 - M_K^2)^2}{8(m_b - m_s)^2} |f_0(q^2)|^2 |C_{\text{SL}} + C_{\text{SR}}|^2 \\ & \left. + \frac{2\lambda_{BK}}{3(M_B + M_K)^2} |f_T(q^2)|^2 |C_{\text{TL}}|^2 \right], \end{aligned} \quad (7)$$

where M_B, M_K are the masses of the B meson and the kaon, respectively, m_b and m_s are the masses of the b and s quarks in the $\overline{\text{MS}}$ scheme, respectively, $\lambda_{BK} \equiv \lambda(M_B^2, M_K^2, q^2)$ is the Källén function, G_F is the Fermi constant, α is the fine structure constant, τ_B is the lifetime of the B meson, and V_{ij} are the Cabibbo-Kobayashi-Maskawa quark mixing matrix elements. The hadronic matrix elements are described by three independent hadronic form factors $f_+(q^2)$, $f_0(q^2)$ and $f_T(q^2)$. The complex-valued Wilson coefficients $C_{\gamma\delta}$ represent the couplings of each contributing operator, where γ stands for vector (V), scalar (S), and tensor (T) operators, respectively, and δ represent left- (L) or right-handed (R) fields. Due to sensitivity to only the absolute values of the three linear combinations of Wilson coefficients, this analysis treats each linear combination as a real-valued number. When using the WET formalism as in Ref. [1], the only non-zero operator in the SM is $C_{\text{VL}}^{\text{SM}} = 6.6 \pm 0.1$ [4]. In this reinterpretation study, the form factors are parametrized following the

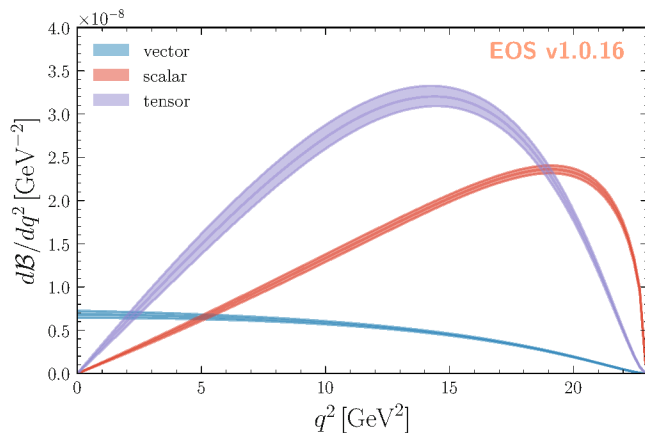


Figure 2. The $B^+ \rightarrow K^+ \nu \bar{\nu}$ differential branching fraction prediction from Eq. (7). Individual contributions are shown here with the combinations of vector, scalar and tensor Wilson coefficients set to unity, respectively. The uncertainties shown (bands) stem from the hadronic parameters.

BSZ parametrization [27], which is truncated at the second order. The eight resulting hadronic parameters are obtained from a joint theoretical prior probability density function (PDF) comprised of the 2021 lattice world average based on results by the Fermilab/MILC and HPQCD collaborations [11, 28]. Theoretical predictions are obtained from the EOS software [29, 30]. The predicted kinematic distributions of the respective vector, scalar and tensor operators are shown in Fig. 2.

To obtain a marginal posterior for the WET Wilson coefficients, we introduce 11 additional parameters to the $B^+ \rightarrow K^+ \nu \bar{\nu}$ statistical model. These include three unconstrained parameters of interest,

$$\eta = [C_{VL} + C_{VR}, C_{SL} + C_{SR}, C_{TL}], \quad (8)$$

along with eight nuisance parameters that parameterize the hadronic form factors. The latter set comprises 8 correlated parameters, which are decorrelated using the eigendecomposition of their covariance matrix (see App. B of Ref. [1]). The three nuisance parameters for the hadronic parameters entering the SM prediction, which were already present in the statistical model, are removed to avoid double counting. We exploit the symmetry of Eq. (7) and sample only in the octant of the parameter space where all Wilson coefficients are positive, and symmetrize the samples afterward. To this end, we choose uniform priors for all Wilson coefficients in the range $[0, 20]$, in the chosen parametrization. Uniform priors are justified by neither wanting to assign preference to any part of the parameter space, nor anticipating inference based on a non-linear transformation of the Wilson coefficients in this study. Ranges are chosen to cover the full posterior. The marginal posterior is shown in Fig. 3. There is a clear deviation from the SM in the vector sector, as expected from the result of Ref. [2]. Further, we find that the posterior distribution peaks around a non-zero value for the tensor contribution. This indicates that a pure SM signal template does not provide the

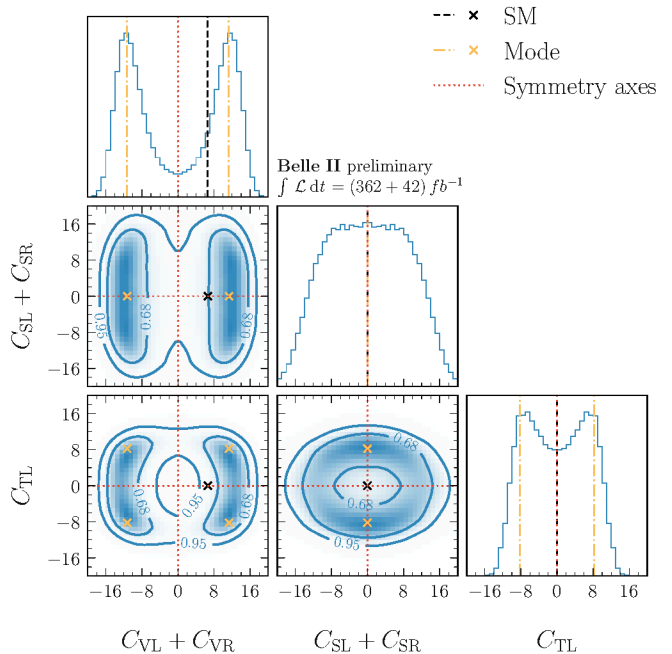


Figure 3. The marginalized posterior for the Wilson coefficients in Eq. (7). We adopt the convention that $C_{VL} + C_{VR}$, $C_{SL} + C_{SR}$ and C_{TL} are real valued. Diagonal and off-diagonal panels show the 1-dimensional and 2-dimensional sample density PDFs on a linear scale, respectively. The overall scale is omitted, as all relevant information is contained in the shape of the distribution. The contours indicate 68% and 95% credible intervals. The dashed black lines and cross mark the SM point; the dash-dotted yellow lines and cross indicate the posterior mode; dotted red lines mark the symmetry axes used for sample symmetrization.

best description of the data (see Appendix A). From the 1-dimensional marginal posterior distributions, we can calculate the highest density credible intervals (HDI)³ at 68% and 95% probability on the absolute values of the Wilson coefficients. The posterior mode and the credible intervals are shown in Table I.

Table I. The mode of the posterior, and HDI at 68% and 95% for the (sums of the) WET Wilson coefficients in Eq. (7), derived from the posterior in Fig. 3.

Parameters	Mode	68% HDI	95% HDI
$ C_{VL} + C_{VR} $	11.3	[7.82, 14.6]	[1.86, 16.2]
$ C_{SL} + C_{SR} $	0.00	[0.00, 9.58]	[0.00, 15.4]
$ C_{TL} $	8.21	[2.29, 9.62]	[0.00, 11.2]

To provide a baseline for comparison, we assess the effect of neglecting kinematic shape information by computing credible intervals using a simplified reinterpretation approach. Technically, this is implemented by

³ The smallest possible credible interval at a given probability level.

performing inference with a likelihood constructed from joint number densities defined over a single bin in the kinematic range, thereby discarding differential distribution information. Within this naive framework, the resulting 95% credible intervals are $|C_{VL} + C_{VR}| < 14.4$, $|C_{SL} + C_{SR}| < 8.51$ and $|C_{TL}| < 7.08$. These values show a bias arising from the assumption that kinematic shape differences can be neglected, as evidenced by the discrepancies relative to the results reported in Table I. The significant variations of the inferred intervals highlight the necessity for reinterpretation approaches, which take these kinematic shape differences into account.

A prior sensitivity analysis was performed to assess the dependence of the presented results on the chosen priors (see Appendix B). Two alternative prior choices were considered. The most stable parameter was found to be $|C_{VL} + C_{VR}|$, while the largest variations occurred for $|C_{SL} + C_{SR}|$, due to the low sensitivity of the analysis to this parameter.

We compare the goodness of fit and relative performance of the WET and the unconstrained $B^+ \rightarrow K^+ \nu \bar{\nu}$ SM, where the signal strength parameter μ_{SM} is treated as a free parameter. To assess relative performance, these models are evaluated against the background-only (BKG) hypothesis, which assumes no $B^+ \rightarrow K^+ \nu \bar{\nu}$ contribution, and the constrained $B^+ \rightarrow K^+ \nu \bar{\nu}$ SM, where μ_{SM} is fixed to the SM prediction. The constrained model includes a 5% normalization uncertainty, which accounts for a 4.4% uncertainty in the CKM matrix elements $|V_{ts}^* V_{tb}|^2$ and a 2.3% uncertainty in $|C_{VL}^{SM}|^2$ [4].

A detailed summary of the models and their defining characteristics is provided in Table II.

Table II. A summary of the models under consideration, their corresponding theoretical predictions, references for the hadronic parameters, and the number of hadronic parameters included in each model is provided.

Model	Prediction	Hadronic Params.	
		Ref.	Nr.
WET	Eq. (7)	[11, 28]	8
SM unconstrained	Eq. (7), $C_{VL} \geq 0$ $C_{\gamma\delta} = 0$ otherwise	[11]	3
SM constrained	Eq. (7), $C_{VL} = 6.6$, $C_{\gamma\delta} = 0$ otherwise, 5% norm. unc.	[11]	3
BKG	no signal	–	–

A local goodness-of-fit (gof) P -value is calculated from

$$P_{\text{gof}} = \int_{\lambda_{\text{obs}}}^{\infty} d\lambda p(\lambda), \quad \lambda = -2 \ln \frac{p(\mathbf{n}, \mathbf{a} | \hat{\boldsymbol{\eta}}, \hat{\boldsymbol{\chi}})}{p_{\text{sat}}(\mathbf{n}, \mathbf{a} | \bar{\boldsymbol{\chi}})}, \quad (9)$$

where $\hat{\boldsymbol{\eta}}, \hat{\boldsymbol{\chi}}$ is the best fit point, and $p_{\text{sat}}(\mathbf{n}, \mathbf{a} | \bar{\boldsymbol{\chi}})$ is the saturated likelihood, where the expected event rates of

the **Histfactory** likelihood [19] are set to the observed data, with all constraint terms maximized at $\bar{\boldsymbol{\chi}}$. The PDF of the test statistic $p(\lambda)$ is obtained from fits to toy data,⁴ sampled from $p(\mathbf{n}, \mathbf{a} | \hat{\boldsymbol{\eta}}, \hat{\boldsymbol{\chi}})$. The goodness of fit P -values are reported in Table III, indicating good fits for all models.

A global model comparison is performed using the Bayes factor, defined as the ratio of the marginal likelihoods between two competing models. The computed Bayes factors are presented in Table III. Both models exceed Jeffreys' condition [32] for a *very strong* model preference ($\log_{10} B > 1.5$) over the background-only hypothesis. Furthermore, both models surpass the threshold for a *substantial* model preference ($\log_{10} B > 0.5$) over the constrained $B^+ \rightarrow K^+ \nu \bar{\nu}$ SM.

Table III. The Bayes factors of each model over the background (constrained $B^+ \rightarrow K^+ \nu \bar{\nu}$ SM) hypothesis, $B_{\text{BKG}} (B_{\text{SM}}^{\text{constr.}})$, and the goodness of fit P -values.

Model	$\log_{10} B_{\text{BKG}}$	$\log_{10} B_{\text{SM}}^{\text{constr.}}$	P_{gof}
WET	1.8	0.68	0.63
SM unconstrained	2.0	0.92	0.58

To support the conclusions derived from the Bayes factor results in Table III, a hypothesis test was conducted using the P -value

$$P = \int_{\lambda_{\text{obs}}}^{\infty} d\lambda p(\lambda), \quad \lambda = -2 \ln \frac{p(\mathbf{n}, \mathbf{a} | \boldsymbol{\eta} = \mathbf{0}, \hat{\boldsymbol{\chi}})}{p(\mathbf{n}, \mathbf{a} | \hat{\boldsymbol{\eta}}, \hat{\boldsymbol{\chi}})}, \quad (10)$$

as a frequentist measure of comparison. The test compares the model at the best fit point $\hat{\boldsymbol{\eta}}, \hat{\boldsymbol{\chi}}$ to the model at the best fit point $\hat{\boldsymbol{\chi}}$ under the condition $\boldsymbol{\eta} = \mathbf{0}$, corresponding to the background-only hypothesis. The distribution of the test statistic $p(\lambda)$ is obtained from fits to toy data, sampled from $p(\mathbf{n}, \mathbf{a} | \boldsymbol{\eta} = \mathbf{0}, \hat{\boldsymbol{\chi}})$. For the WET we obtain a P -value of $P = 4.6 \cdot 10^{-4}$, corresponding to a significance of $Z = 3.3$, over the background-only hypothesis. This is smaller than the $Z = 3.5$ obtained in Ref. [2] due to the increased number of model parameters and the updated form factor parametrization.

In conclusion, this letter describes a robust reinterpretation of the $B^+ \rightarrow K^+ \nu \bar{\nu}$ result [2] within the WET, using the model-agnostic likelihood approach. From the analysis likelihood, in conjunction with only the joint number densities, we construct Bayesian posterior models, and derive marginal posteriors as well as credible intervals on theoretical model parameters. We present the first reported credible intervals on the $b \rightarrow s$ WET Wilson coefficients, from a thorough reinterpretation of Belle II data in Table I. In summary, the posterior mode for the magnitudes

⁴ Note that for the WET, $p(\lambda)$ does not follow the asymptotic chi-square distribution, as the Wilson coefficients can only positively contribute to the rate in Eq. (7) (for a discussion see Ref. [31]).

of the Wilson coefficient combinations is found at $(|C_{VL} + C_{VR}|, |C_{SL} + C_{SR}|, |C_{TL}|) = (11.3, 0.00, 8.21)$, with corresponding 95% credible intervals of $[1.86, 16.2]$, $[0.00, 15.4]$, and $[0.00, 11.2]$, respectively. We find that an enhancement in the vector sector is required to obtain good compatibility with the data. However, the best overall compatibility is achieved with an additional, sizable tensor contribution.

A central goal of this work is to enable broad reinterpretation of the $B^+ \rightarrow K^+ \nu \bar{\nu}$ measurement by publishing the model-agnostic likelihood, which consists of the full likelihood from the $B^+ \rightarrow K^+ \nu \bar{\nu}$ result [2] and the joint number densities used in this reinterpretation [33] (for details see Appendix C). This allows the broader scientific community to test alternative theoretical models in a statistically rigorous way. Importantly, this publication sets a template for future Belle II measurements that are suitable for reinterpretation and reflects the collaboration's commitment to publish model-agnostic likelihoods as a means to maximize the scientific impact and reusability of its results.

This work, based on data collected using the Belle II detector, which was built and commissioned prior to March 2019, was supported by Higher Education and Science Committee of the Republic of Armenia Grant No. 23LCG-1C011; Australian Research Council and Research Grants No. DP200101792, No. DP210101900, No. DP210102831, No. DE220100462, No. LE210100098, and No. LE230100085; Austrian Federal Ministry of Education, Science and Research, Austrian Science Fund (FWF) Grants DOI: 10.55776/P34529, DOI: 10.55776/J4731, DOI: 10.55776/J4625, DOI: 10.55776/M3153, and DOI: 10.55776/PAT1836324, and Horizon 2020 ERC Starting Grant No. 947006 “InterLeptons”; Natural Sciences and Engineering Research Council of Canada, Compute Canada and CANARIE; National Key R&D Program of China under Contract No. 2024YFA1610503, and No. 2024YFA1610504 National Natural Science Foundation of China and Research Grants No. 11575017, No. 11761141009, No. 11705209, No. 11975076, No. 12135005, No. 12150004, No. 12161141008, No. 12475093, and No. 12175041, and Shandong Provincial Natural Science Foundation Project ZR2022JQ02; the Czech Science Foundation Grant No. 22-18469S, Regional funds of EU/MEYS: OPJAK FORTE CZ.02.01.01/00/22_008/0004632 and Charles University Grant Agency project No. 246122; European Research Council, Seventh Framework PIF-GA-2013-622527, Horizon 2020 ERC-Advanced Grants No. 267104 and No. 884719, Horizon 2020 ERC-Consolidator Grant No. 819127, Horizon 2020 Marie Skłodowska-Curie Grant Agreement No. 700525 “NIOBE” and No. 101026516, and Horizon 2020 Marie Skłodowska-Curie RISE project JENNIFER2 Grant Agreement No. 822070 (European grants); L’Institut National de Physique Nucléaire et de Physique des Particules (IN2P3) du CNRS and L’Agence Nationale de la Recherche (ANR) under Grant

No. ANR-21-CE31-0009 (France); BMFTR, DFG, HGF, MPG, and AvH Foundation (Germany); Department of Atomic Energy under Project Identification No. RTI 4002, Department of Science and Technology, and UPES SEED funding programs No. UPES/R&D-SEED-INFRA/17052023/01 and No. UPES/R&D-SOE/20062022/06 (India); Israel Science Foundation Grant No. 2476/17, U.S.-Israel Binational Science Foundation Grant No. 2016113, and Israel Ministry of Science Grant No. 3-16543; Istituto Nazionale di Fisica Nucleare and the Research Grants BELLE2, and the ICSC – Centro Nazionale di Ricerca in High Performance Computing, Big Data and Quantum Computing, funded by European Union – NextGenerationEU; Japan Society for the Promotion of Science, Grant-in-Aid for Scientific Research Grants No. 16H03968, No. 16H03993, No. 16H06492, No. 16K05323, No. 17H01133, No. 17H05405, No. 18K03621, No. 18H03710, No. 18H05226, No. 19H00682, No. 20H05850, No. 20H05858, No. 22H00144, No. 22K14056, No. 22K21347, No. 23H05433, No. 26220706, and No. 26400255, and the Ministry of Education, Culture, Sports, Science, and Technology (MEXT) of Japan; National Research Foundation (NRF) of Korea Grants No. 2021R1-F1A-1064008, No. 2022R1-A2C-1003993, No. 2022R1-A2C-1092335, No. RS-2016-NR017151, No. RS-2018-NR031074, No. RS-2021-NR060129, No. RS-2023-00208693, No. RS-2024-00354342 and No. RS-2025-02219521, Radiation Science Research Institute, Foreign Large-Size Research Facility Application Supporting project, the Global Science Experimental Data Hub Center, the Korea Institute of Science and Technology Information (K25L2M2C3) and KREONET/GLORIAD; Universiti Malaya RU grant, Akademi Sains Malaysia, and Ministry of Education Malaysia; Frontiers of Science Program Contracts No. FOINS-296, No. CB-221329, No. CB-236394, No. CB-254409, and No. CB-180023, and SEP-CINVESTAV Research Grant No. 237 (Mexico); the Polish Ministry of Science and Higher Education and the National Science Center; the Ministry of Science and Higher Education of the Russian Federation and the HSE University Basic Research Program, Moscow; University of Tabuk Research Grants No. S-0256-1438 and No. S-0280-1439 (Saudi Arabia), and Researchers Supporting Project number (RSPD2025R873), King Saud University, Riyadh, Saudi Arabia; Slovenian Research Agency and Research Grants No. J1-50010 and No. P1-0135; Ikerbasque, Basque Foundation for Science, State Agency for Research of the Spanish Ministry of Science and Innovation through Grant No. PID2022-136510NB-C33, Spain, Agencia Estatal de Investigación, Spain Grant No. RYC2020-029875-I and Generalitat Valenciana, Spain Grant No. CIDEAGENT/2018/020; The Knut and Alice Wallenberg Foundation (Sweden), Contracts No. 2021.0174 and No. 2021.0299; National Science and Technology Council, and Ministry of Education (Taiwan); Thailand Center of Excellence in Physics;

TUBITAK ULAKBIM (Turkey); National Research Foundation of Ukraine, Project No. 2020.02/0257, and Ministry of Education and Science of Ukraine; the U.S. National Science Foundation and Research Grants No. PHY-1913789 and No. PHY-2111604, and the U.S. Department of Energy and Research Awards No. DE-AC06-76RLO1830, No. DE-SC0007983, No. DE-SC0009824, No. DE-SC0009973, No. DE-SC0010007, No. DE-SC0010073, No. DE-SC0010118, No. DE-SC0010504, No. DE-SC0011784, No. DE-SC0012704, No. DE-SC0019230, No. DE-SC0021274, No. DE-SC0021616, No. DE-SC0022350, No. DE-SC0023470; and the Vietnam Academy of Science and Technology (VAST) under Grants No. NVCC.05.12/22-23 and No. DL0000.02/24-25.

These acknowledgements are not to be interpreted as an endorsement of any statement made by any of our institutes, funding agencies, governments, or their representatives.

We thank the SuperKEKB team for delivering high-luminosity collisions; the KEK cryogenics group for the efficient operation of the detector solenoid magnet and IBelle on site; the KEK Computer Research Center for on-site computing support; the NII for SINET6 network support; and the raw-data centers hosted by BNL, DESY, GridKa, IN2P3, INFN, and the University of Victoria.

Appendix A: Predicted yields at the posterior mode

Direct comparison of the observed data yields to the predicted yields at the posterior mode parameter point (the best fit point to data; see Table I) for the unconstrained $B^+ \rightarrow K^+ \nu \bar{\nu}$ SM and the WET is shown in Fig. 4, for the highest-sensitivity bins of the analysis. The WET model provides a better fit to the data than the unconstrained SM prediction, as indicated by the smaller pull values.

Appendix B: Prior sensitivity study

To investigate the sensitivity of the results in Table I to the choice of priors, we derived the posterior mode and credible intervals for alternative sets of priors.

Firstly, we select truncated-normal priors, centered on the SM expectation (the only non-zero Wilson coefficient being $C_{VL}^{\text{SM}} = 6.6$), which disfavor deviations from the SM expectation,

$$p(\eta_i) = \begin{cases} \mathcal{N}(\eta_i | \mu = C_i^{\text{SM}}, \sigma = 20) & \eta_i \geq 0 \\ 0 & \eta_i < 0 \end{cases}. \quad (\text{B1})$$

Here $\eta_i \in [|C_{VL} + C_{VR}|, |C_{SL} + C_{SR}|, |C_{TL}|]$ and C_i^{SM} correspond to the respective SM point $C_i^{\text{SM}} \in [6.6, 0.0, 0.0]$.

Secondly, we select uniform priors in the squared Wilson coefficients, as these enter Eq. (7), which subse-

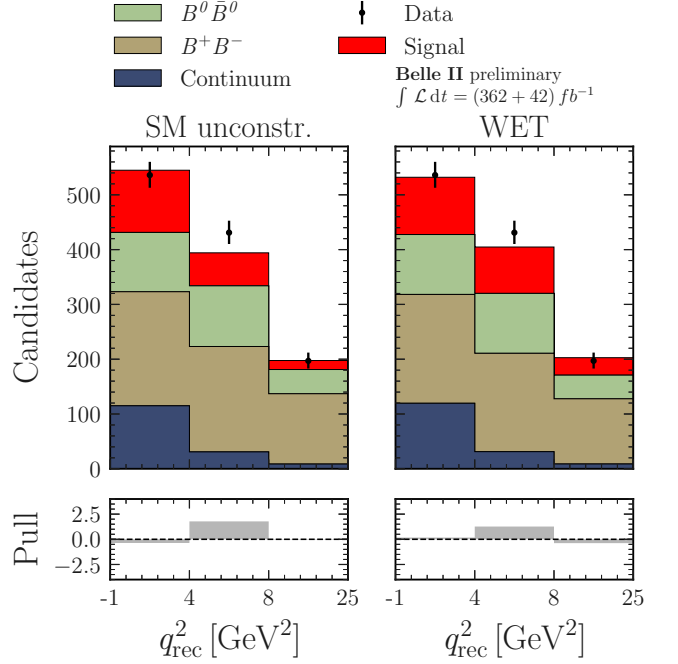


Figure 4. Observed and predicted best fit yields in the high-sensitivity bins of the analysis. These correspond to the $\eta(\text{BDT}_2) > 0.98$ region of the ITA. The signal is shown for the unconstrained $B^+ \rightarrow K^+ \nu \bar{\nu}$ SM (left) and the WET (right) predictions. The predicted background yields are shown individually for the neutral and charged B -meson decays, and the summed five continuum categories. Pulls are shown in the lower panels.

quently translate to linear priors for the Wilson coefficients,

$$p(\eta_i) \propto \begin{cases} \eta_i & \eta_i \leq 30 \\ 0 & \eta_i > 30 \end{cases}. \quad (\text{B2})$$

These priors favor larger values for the Wilson coefficients.

The resulting credible intervals for both cases are shown in Table IV. The vector Wilson coefficient posterior mode and credible intervals are found to be the most robust to prior choices. The largest changes are found for the scalar Wilson coefficients, which the analysis is the least sensitive to, due to low efficiency at high q^2 . This is also expected from the posterior distribution in Fig. 3.

Appendix C: Belle II HEPData reinterpretation inventory

To enable reinterpretation under any NP model with the model-agnostic likelihood [1], the necessary information from Belle II will be published on HEPData [33]. The release will include the following components:

- The SM $B^+ \rightarrow K^+ \nu \bar{\nu}$ differential branching fraction as a function of q^2 ;

Table IV. The posterior modes, and HDIs at 68% and 95% for the (sums of the) WET Wilson coefficients in Eq. (7), for alternative prior choices (cf. Table I).

Priors	Parameters	Mode	68% HDI	95% HDI
Eq. (B1)	$ C_{VL} + C_{VR} $	11.4	[7.97, 14.6]	[2.21, 16.4]
	$ C_{SL} + C_{SR} $	0.00	[0.00, 9.16]	[0.00, 14.7]
	$ C_{TL} $	7.69	[1.54, 8.75]	[0.00, 11.0]
Eq. (B2)	$ C_{VL} + C_{VR} $	11.6	[8.21, 14.0]	[4.17, 16.0]
	$ C_{SL} + C_{SR} $	8.93	[4.56, 12.6]	[1.27, 15.6]
	$ C_{TL} $	7.17	[3.86, 9.59]	[1.41, 11.7]

- Signal selection efficiency as a function of q^2 ;

- Binned joint number densities:

- ITA: x-axis: q^2 , y-axis: $q_{\text{rec}}^2 \times \eta(\text{BDT}_2)$ (flattened), z-axis: events (weighted);
- HTA: x-axis: q^2 , y-axis: $\eta(\text{BDTh})$ (flattened), z-axis: events (weighted);

- pyhf combined likelihood in json format:

- Containing templates for signal and background after all selections, binned in $q_{\text{rec}}^2 \times \eta(\text{BDT}_2)$ (ITA) and $\eta(\text{BDTh})$ (HTA);

- The code to reproduce the WET reinterpretation results obtained in this analysis.

-
- [1] L. Gärtner, N. Hartmann, L. Heinrich, M. Horstmann, T. Kuhr, M. Reboud, S. Stefkova, and D. van Dyk, *Eur. Phys. J. C* **84**, 693 (2024).
 - [2] I. Adachi *et al.* (Belle II Collaboration), *Phys. Rev. D* **109**, 112006 (2024).
 - [3] S. L. Glashow, J. Iliopoulos, and L. Maiani, *Phys. Rev. D* **2**, 1285 (1970).
 - [4] W. G. Parrott, C. Bouchard, and C. T. H. Davies (HPQCD collaboration), *Phys. Rev. D* **107**, 014511 (2023).
 - [5] T. E. Browder *et al.* (CLEO Collaboration), *Phys. Rev. Lett.* **86**, 2950 (2001).
 - [6] O. Lutz *et al.* (Belle Collaboration), *Phys. Rev. D* **87**, 111103 (2013).
 - [7] J. P. Lees *et al.* (BABAR Collaboration), *Phys. Rev. D* **87**, 112005 (2013).
 - [8] P. del Amo Sanchez *et al.* (BABAR Collaboration), *Phys. Rev. D* **82**, 112002 (2010).
 - [9] J. Grygier *et al.* (Belle Collaboration), *Phys. Rev. D* **96**, 091101 (2017).
 - [10] F. Abudinén *et al.* (Belle II Collaboration), *Phys. Rev. Lett.* **127**, 181802 (2021).
 - [11] W. G. Parrott, C. Bouchard, and C. T. H. Davies (HPQCD collaboration), *Phys. Rev. D* **107**, 014510 (2023).
 - [12] K. Fridell, M. Ghosh, T. Okui, and K. Tobioka, *Phys. Rev. D* **109**, 115006 (2024).
 - [13] W. Altmannshofer, A. Crivellin, H. Haigh, G. Inguglia, and J. M. Camalich, *Phys. Rev. D* **109**, 075008 (2024).
 - [14] E. Gabrielli, L. Marzola, K. Mürsepp, and M. Raidal, *Eur. Phys. J. C* **84**, 460 (2024).
 - [15] D. Bečirević, I. Doršner, S. Fajfer, D. A. Faroughy, N. Košnik, and O. Sumensari, *Phys. Rev. D* **98**, 055003 (2018).
 - [16] T. E. Browder, N. G. Deshpande, R. Mandal, and R. Sinha, *Phys. Rev. D* **104**, 053007 (2021).
 - [17] J. M. Camalich, M. Pospelov, P. N. H. Vuong, R. Ziegler, and J. Zupan, *Phys. Rev. D* **102**, 015023 (2020).
 - [18] A. Filimonova, R. Schäfer, and S. Westhoff, *Phys. Rev. D* **101**, 095006 (2020).
 - [19] K. Cranmer, G. Lewis, L. Moneta, A. Shibata, and W. Verkerke (ROOT), *HistFactory: A tool for creating statistical models for use with RooFit and RooStats*, Tech. Rep. (New York U., New York, 2012).
 - [20] L. Heinrich, M. Feickert, and G. Stark, *scikit-hep/pyhf*: v0.7.6 (2024), see also the GitHub webpage.
 - [21] L. Heinrich, M. Feickert, G. Stark, and K. Cranmer, *J. Open Source Software* **6**, 2823 (2021).
 - [22] L. Gärtner, *lorenzennio/redist*: redist version 1.0.4 (2025), see also the GitHub webpage.
 - [23] Feickert, Matthew, Heinrich, Lukas, and Horstmann, Malin, *EPJ Web of Conf.* **295**, 06004 (2024).
 - [24] O. Abril-Pla, V. Andreani, C. Carroll, L. Dong, C. J. Fonnesbeck, M. Kochurov, R. Kumar, J. Lao, C. C. Luhmann, O. A. Martin, *et al.*, *PeerJ Computer Science* **9** (2023).
 - [25] T. Felkl, S. L. Li, and M. A. Schmidt, *J. High Energ. Phys.* **12**, 118.
 - [26] J. Gratrex, M. Hopfer, and R. Zwicky, *Phys. Rev. D* **93**, 054008 (2016).
 - [27] A. Bharucha, D. M. Straub, and R. Zwicky, *J. High Energ. Phys.* **08**, 098.
 - [28] Y. Aoki *et al.* (Flavour Lattice Averaging Group (FLAG)), *Eur. Phys. J. C* **82**, 869 (2022).
 - [29] D. van Dyk *et al.* (EOS Authors), *Eur. Phys. J. C* **82**, 569 (2022).
 - [30] D. van Dyk, M. Reboud, M. Kirk, N. Gubernari, P. Lüghausen, F. Herren, D. Leljak, S. Kürten, A. Kokulu, C. Bolognani, *et al.*, *eos/eos*: EOS version 1.10.16 (2025), see also the GitHub webpage.
 - [31] F. U. Bernlochner, D. C. Fry, S. B. Menary, and E. Persson, *SciPost Phys. Core* **6**, 013 (2023).
 - [32] H. Jeffreys, *The Theory of Probability*, 3rd ed. (Oxford University Press, 1961).
 - [33] Belle II Collaboration, To follow after journal submission, HEPData (collection).